PHYSICAL REVIEW B **87**, 245424 (2013)

Hybrid particle-in-cell/molecular dynamics simulation of swift-ion tracks in LiF

Yaroslav Cherednikov, Si Neng Sun, and Herbert M. Urbassek*
Fachbereich Physik und Forschungszentrum OPTIMAS, Universität Kaiserslautern, Erwin-Schrödinger-Straße, D-67663 Kaiserslautern, Germany

(Received 5 April 2013; published 21 June 2013)

We model the processes induced in a LiF crystal by a swift ion. The impinging ion creates an ionization cylinder of doubly ionized F^+ ions, while simultaneously the corresponding electrons are set free. Ions move according to molecular dynamics, while excited electrons are treated by a particle-in-cell scheme. We treat the recombination time of electrons as a free parameter in our model. Electrons are found to partially shield the ions in the track; the shielding is, however, minor (10% on the average), and occurs mainly in the first 50 fs of the process. We characterize the ion track formed inside the target; it consists of underdense (60% of the initial density), highly defective material. Within the first 50 fs, a Coulomb explosion is seen in the ion trail. Its most prominent effect is the emission of fast (7–8 eV) Li^+ ions from the solid. It is caused by electrical fields at the target surface of the order of 10^{10} V/m.

DOI: 10.1103/PhysRevB.87.245424 PACS number(s): 61.80.Az, 79.20.Ap, 52.65.Rr, 78.55.Hx

I. INTRODUCTION

The interaction of swift ions—defined as ions with energies around or above the maximum of the electronic stopping power—with matter has been a subject of intense study since the early days of nuclear physics. The creation of ion tracks—lasting damage in the target along the trail of the swift ion—formed a topic of prominent interest.[1] These are regions of modified material—typically molten and refrozen or amorphized—extending along the straight ion trajectory into the solid; their shape is cylindrical with radii of a few nm, depending on the ion species and energy, and the target material. In addition, swift ions induce sputtering from the surface.[2] Among the materials investigated, alkali halides, and in particular LiF, are subject to particularly abundant sputtering.[3]

The mechanisms involved in the formation of swift-ion tracks are complex.[4,5] The projectile swift ion deposits its energy in the form of electronic excitation along the ion trail, and as primary fast electrons (so-called δ electrons), which leave the ionization cylinder and deposit their energy in the surroundings. The fast electrons will eventually thermalize and energy is given to the atomic lattice, which then may form a measurable track structure.

The modeling of the processes occurring in swift-ion tracks is far from complete. The energy deposition (electronic stopping) by the swift ion along its path has long been understood, in particular for energies far above the electronic stopping power maximum.[6] But more recently, also the region around the stopping power maximum, where electron capture and loss from and to the projectile become important, is more reliably understood.[7] The physics of electron transport around the ionization region and the slowing down and secondary cascades of electrons have been modeled by Monte Carlo recipes, such that the temporal and radial structure of energy deposition in the electronic system around the ionization trail are understood.[8–10]

Starting in the early 1990s, atomistic simulation was employed to model the processes occurring in the atomic system, such as the formation of a radial pressure wave, density reduction along the center of the ionization cylinder, material melting and evaporation, and sputtering phenomena.[11–13] In such simulations, the primary excitation process was simplified by assuming that the excitation energy is directly given to the atomic system; in this way, the modeling of the electronic system enters as an initial condition to the atom dynamics and need not be separately modeled. Such simulations have been originally performed on generic materials (modeled by a Lennard-Jones potential), and more recently have been expanded to realistic materials, in particular silica.[14–16] In such simulations, it is comparatively easy to include the effects of the temporal and radial structure of the electronic excitation.[17,18]

Few simulations have been performed up to now in which the ions created in the track core have been taken into account. Due to the strong positive charge of the track core—a consequence of the leaving electrons—these ions may lead to a *Coulomb explosion*, in which the electrostatic energy is used for track formation and particle emission.[1,19] The physics underlying Coulomb explosion and the extent to which it contributes to sputtering from tracks are still under discussion.[5,20]

In all previous simulations of ion tracks, the electronic and atomic systems were modeled separately. In the present approach we want to go beyond this stage and study the interplay of electronic and atomic systems. This is possible in a hybrid algorithm which simulates the time evolution of atoms and of electrons in separate schemes; however, after each time step information between the schemes is exchanged. This allows us to study the interplay between electron and atom evolution, and to answer questions such as to the screening of ions by electrons or the generation of electrical fields and their effect. This will be possible in a self-consistent way.

Up to now, only a few, if any, simulations have been performed on swift-ion tracks in ionic solids, such as the alkali halides. A notable exception is given by the work of Young who performed molecular dynamics simulations of the Coulomb explosion in KCl, LiF, and CaF_2 crystallites.[21–23] Ionic charges are omnipresent in ionic solids and are decisive for modeling the materials properties. In addition, as in any other solid, the penetrating swift ion will induce further ionization and

©2013 American Physical Society

free electrons in the system; thus the balance of local charge neutrality in each unit cell will be disturbed. The resulting long-range forces may be important for track physics and sputtering. Indeed, as mentioned above, in these systems, the largest sputter yields have been observed. It also seems that in these systems the influence of a Coulomb explosion will be most clearly seen, since charges will never be fully quenched.

The study of ion interaction with ionic solids has received further interest due to their use as containers for radioactive waste.[24] Here the effects of both high-energy fission fragments and of lower (keV) energy recoil atoms—mainly from α-particle emission—are of interest. Up to now, simulation studies in this area have concentrated mostly on the keV regime, thus excluding electronic effects and the study of ion tracks, and concentrated on the effects in ceramics and minerals.[25–28] A further interesting application is given by the interaction of cosmic rays with interstellar dust particles.[29] Here the role of ion tracks is to phase-transform initially crystalline dust grains to an amorphous structure.

We present here a model study which focuses on the early stages of energy deposition in the atomic system. A preliminary study concentrating on the induced sputtering from LiF has been submitted elsewhere.[30] We provide the framework of a hybrid simulation scheme which couples a molecular dynamics (MD) scheme for the ionic system with a particle-in-cell scheme (PIC) for the electrons. This allows us to model directly the initial ionization by the swift ion, and the charge screening by the electrons. We do not model electron recombination individually, but rather assume an electron recombination time τ, which we use as a free model parameter. Our model thus allows us to estimate the effects of the additional ion charges, and thus of Coulomb explosion, on the track formation and sputtering.

II. METHOD

We apply a hybrid simulation scheme in which the motion of the ions is calculated using MD, while the properties of the electron system are modeled using PIC.[31–33] In our approach, we treat the electrons as a fluid whose density instantaneously accommodates to the local potential. This allows us to use a larger time step in the simulation; it is adjusted to resolving the ion motion, rather than the electron motion.[34] Below (see discussion of Fig. 6 at the end of Sec. III B) we argue that such a fluid treatment of the electrons is valid after a few fs after swift-ion passage. From the spatial distribution of free electrons we can calculate the screening of the ionic charges—which will modify the Coulomb forces in the MD—and the field distribution in the sample.

The incident swift ion is the source of electron excitation and ionization in the target. We model it by suddenly double-ionizing the F^- ions in the cylindrical ionization cylinder to F^+ ions, and simultaneously generating free electrons at the positions of these ions. This form of ionization is plausible considering the ionization energies, which are 5.4 (17.4) eV for the first and 75.8 (35) eV for the second ionization of Li (F), respectively.

The ensuing dynamics in the target is calculated by considering the forces on the ions (MD) and the redistribution of the electrons (PIC). We do not include a detailed model of electron collisions and the accompanying effects such as impact ionization, Auger decay, or trapping of electrons; such effects would best be modeled in a Monte Carlo simulation such as Refs. 8 and 9. Here, we simplify these processes by assuming a finite lifetime of the electrons, which we shall denote as the recombination time τ. It will be treated as a free parameter of our simulation and vary between 50 and 1000 fs. After this time, we assume all electrons to be recaptured at the F^+ ions; then the MD will proceed as in electronically un-excited LiF, while PIC will be unnecessary since no free electrons are left.

Certainly, in reality, not all F^+ ions will recombine at the same time. We vary the recombination time in the limits given above in order to assess the importance of this parameter. However, we point out that some color centers (in our case neutral F^0 atoms) may be formed and remain in the target; we do not take these into account in the present model.

In general the electron dynamics during the ionization phase is governed by (i) their kinetic energy, (ii) the track potential, (iii) possible traps for electrons, and (iv) recombination. In our model, we take (ii) fully into account, and (i) and (iv) in terms of model parameters (electron temperature and recombination time, respectively), while the existence of traps is ignored.

We note that the method presented here has been set up to describe the processes occurring in an insulating target, but will not be suitable for metals.

A. Particle-in-cell scheme

We implemented a 3-dimensional electrostatic microscopic particle-in-cell scheme (ES-MPIC) with a discretization size of 1 Å. Such schemes have been used previously to calculate the electron dynamics in laser-irradiated clusters.[35,36] This PIC cell size is considerably smaller than the lattice constant of LiF, $a = 4.026$ Å. PIC allows us to calculate the electron density distribution, as well as the electrical potential and field throughout the simulation volume. The electron density determined by PIC is used for screening the ionic charges in the MD code.

We consider electrons as a classical fluid with their local density given by the Boltzmann relationship,

$$n_e = n_0 \exp\left[\frac{e(\phi - \phi_0)}{k_B T_e}\right], \tag{1}$$

where ϕ is the electric potential, n_e is the electron density, e is the elementary charge, and k_B is Boltzmann's constant. We assume the electron temperature, T_e, to be constant throughout our simulation. The electric potential is given by the Poisson equation,

$$\nabla^2\phi = -\frac{\rho}{\varepsilon_0}, \tag{2}$$

where ρ is the charge density and ε_0 is the vacuum permittivity. The charge density is calculated via

$$\rho = e(Z_i n_i - n_e) \tag{3}$$

from the electron density n_e, the ion density n_i, and the nominal ion charge Z_i. We implement Dirichlet boundary conditions for PIC such that the potential is zero on the boundaries.

Ideally, these equations should be supplemented by an equation for the time and space evolution of the electron temperature. Such an equation has been used for example to describe the temperature evolution in laser-irradiated LiF,[37] and has also been implemented in a hybrid MD code.[38] In that application, however, the space dependence of the electron temperature could be ignored; this is not possible in the present problem. Due to the highly nonlinear character of the plasma equations, this equation is not easily solved in 3 dimensions; we refrain here from implementing it.

We solve the Poisson equation numerically in 3 dimensions using the successive overrelaxation (SOR) method.[39] A time step of 1 fs, identical to that in the MD scheme, is adopted.

B. Molecular dynamics scheme

Lithium and fluorine ions interact by a Buckingham-like potential,

$$V_{ij}(r) = \frac{q_i q_j}{4\pi\epsilon_0 r} + A_{ij}\exp\left(-r/\rho_{ij}\right) - \frac{C_{ij}}{r^6}. \qquad (4)$$

We use the parameters A_{ij} and ρ_{ij} for the F-F, Li-F, and Li-Li core interactions as given by Ref. 22. However, we lowered the value of the van der Waals parameter C_{FF} from 21.367 to 14 eVÅ^6 to avoid the Buckingham collision catastrophe[22] during the ionization stage; the other van der Waals parameters are zero.

The screened ion charges q_i are determined from the nominal ion charge Z_i and the electron density in the appropriate PIC cell via

$$q_i = eZ_i - \Omega n_e, \qquad (5)$$

where Ω is the volume per ion, and n_e is the local electron density averaged over the volume of the ion. This equation incorporates the electron screening as calculated by PIC into the MD scheme.

The potentials are cut off at $r_{\text{cut}} = 0.85$ nm; between 0.75 and 0.85 nm they are smoothly splined to zero using a cosine function.

We employ the velocity Verlet integrator with a time step of 1 fs to solve the equations of motion for the ions. The Coulomb interactions are treated by using an empirical screening potential.[40] The screening parameter in that approach has been set to $\alpha = 0.25$.

C. Data analysis

From the ion trajectories we calculate the local temperature and pressure of all the ions; they are defined as averages over local ensembles as follows. All ions, which are closer than the cutoff distance, r_{cut}, to an ion i form its interaction partners; the ensemble Ω_i of all these interaction partners is used for averaging.

The center-of-mass velocity of the ensemble, $\mathbf{V}_i$, is determined as the average over all individual ion velocities $\mathbf{v}_j$ in the ensemble. The thermal velocity of ion j in the ensemble Ω_i then is $\mathbf{v}'_j = \mathbf{v}_j - \mathbf{V}_i$. The temperature T_i of ion i is determined by the average kinetic energy of the thermal motion in ensemble Ω_i. The local pressure p_i is determined by

$$p_i = \frac{N k_B T_i}{V} + \frac{1}{3V}\sum_{j=1}^{N} \mathbf{r}_{ij}\cdot\mathbf{F}_{ij}, \qquad (6)$$

where N is the number of ions in this ensemble, V is its volume, and $\sum_j \mathbf{r}_{ij}\cdot\mathbf{F}_{ij}$ denotes the interaction virial over all the interacting ions in the ensemble. The first term describes the pressure contribution of the thermal motion; the second term is due to the stress resulting from the interaction. From the local temperatures T_i and the local pressures p_i the distribution of temperature and pressure in the crystal is obtained.

D. System and parameters

LiF has NaCl structure with 4 F$^-$ and 4 Li$^+$ ions per unit cell. The lattice constant of LiF amounts to $a = 4.026$ Å. The volume per ion amounts to $\Omega = a^3/8 = 8.15$ Å^3.

For our simulations we use 3 LiF crystals. They have the form of freestanding ultrathin LiF crystals with dimensions of $20 \times 20 \times 4$, $14 \times 14 \times 8$, and $10 \times 10 \times 16$ unit cells; the last number gives the thickness of the crystal. We shall call these crystals *thin*, *middle*, and *thick*, respectively. They contain approximately the same amount of atoms (12 800, 12 544, 12 800). All crystals have (100) surfaces. We employ free boundary conditions at all 6 sides of our crystallites in our MD scheme. Thus we effectively model ion tracks in a freestanding clusters; this is similar to the approach by Young.[21–23]

The ionization trail is modeled as a cylinder of radius $R = 2$ Å, with its axis perpendicular into the target. We thus assume that the electronic excitation occurs in those atoms that lie on the swift-ion path; the excitation cylinder has a lateral radius roughly equal to the nearest-neighbor distance in LiF. The ionization corresponds to the generation of 2 F$^+$ ions and 4 free electrons per LiF monolayer of width $a/2$. The initial electron density is high, $n_e = 0.16$ Å^{-3}. The energy deposited by the swift ion amounts to the sum of potential energies of the created F$^+$ ions and kinetic energies of the electrons.

The temperature of free electrons is set to $k_B T_e = 8$ eV. This value was taken as the result of several preliminary simulations: If T_e is chosen too large, all electrons leave the target quickly, and they do not affect the further LiF dynamics; if T_e is chosen too small, the electrons remain trapped at the F$^+$ ions from which they originate, and the effect of the ionizing swift ion is not felt. The value of $k_B T_e = 8$ eV adopted by us was found to be intermediate between these two extremes. We note that electron temperatures in swift-ion tracks could be measured experimentally in several targets using Auger electron emission,[5] but up to now not in LiF. These data show that that kT_e is in the range of up to several eV. The exact value depends on the target and the projectile species and energy; our value of 8 eV is in the upper range of measured electron temperatures. Electrons will lose their energy on a time scale of 0.5–1 ps in LiF;[37] while we do not include electron energy loss in our model, our choice of the maximum recombination time of 1 ps guarantees that both ion excitations and electrons play no role in the dynamics of the surface for larger times.

The potential energy needed to double-ionize an F$^-$ ion is given as the sum of the electron affinity, $A = 3.40$ eV, and the ionization energy, $I = 17.42$ eV. Thus per F^+ ion, an energy of 44.82 eV has been invested. In the energized cylinder, we thus obtain an energy density of $e_0 = 3.54\ \text{eV/Å}^3$. This is equivalent to a stopping power of $dE/dx = \pi R^2 e_0 = 44.5$ eV/Å. Such stopping powers are typical of impacts of light ions.[2]

We note that it would be interesting to extend our model to cover higher energy depositions, such as they are typical for swift *heavy* ion impacts. In such a case, however, not only F^+ ions but also higher ionization states of fluorine, and also of lithium, would be created, thus severely complicating the modeling.

Using the stopping power of $dE/dx = 44.5$ eV/Å derived above, an energy of 717 (1433, 2867) eV was deposited in the thin, middle, and large crystals, respectively. If this energy were totally converted to heating the LiF crystal, an end temperature of 217 (442, 867) K would be obtained; here a heat capacity of $3k_B$ per ion was assumed.

The PIC simulation boxes are chosen larger than the LiF crystal sizes; they amount to $120 \times 120 \times 100$, $90 \times 90 \times 160$, and $70 \times 70 \times 240$ Å^3, respectively. The number of PIC cells is thus of the order of 10^6 cells.

The recombination time of free electrons is taken as a model parameter; we performed simulations with $\tau = 50$, 100, 250, 500, and 1000 fs. This is also of the order of the energy relaxation time of the electronic system which determines the time scale of energy exchange with the ionic system in LiF and which has been estimated in Ref. 37 to be around 0.5–1.0 ps.

We relax the LiF crystals for 30 ps; at the start of the simulation they have a temperature of around 10 K. At time $t = 0$, we start the ionization process: For a period of time τ, all F^- ions are converted to F^+; simultaneously in those PIC cells, where an F^+ ion has been created, 2 electrons are inserted. This gives the initial condition for the PIC/MD scheme.

III. RESULTS

A. Ion track

Figure 1 shows in a series snapshots the processes occurring in the target after passage of the swift ion. Temperatures in the ion trail cylinder quickly rise to values well above the melting temperature. The high energy density then leads to strong sputtering from the trail region; emission starts immediately after ionization but persists to times >1 ps. In the final snapshot, at a time of 5 ps after ion passage, the crystal has equilibrated at a temperature of around 800 K. Some material has been deposited loosely on the surface. The track region itself shows a highly defective structure, which will be further discussed below; see Fig. 5. A top view, Fig. 2, reveals a temporary hole forming in the track center, which is due to the radial expansion of the material caused by the huge central energy density.

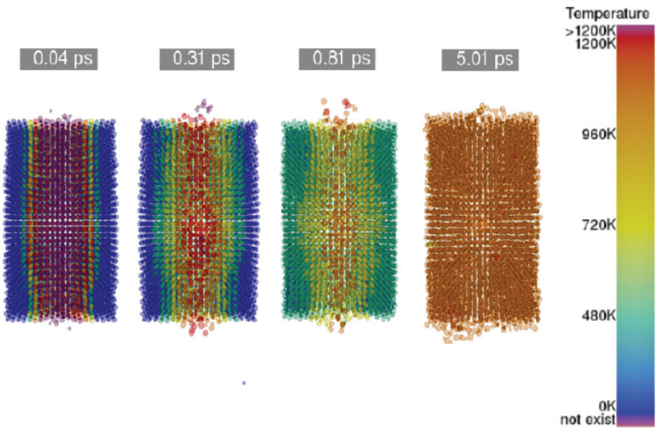

FIG. 1. (Color online) Cross-sectional view through the thick crystallite at times of 40, 310, 810, and 5000 fs after passage of the swift ion. Recombination time $\tau = 1000$ fs. Color codes local temperature, see color bar at right.

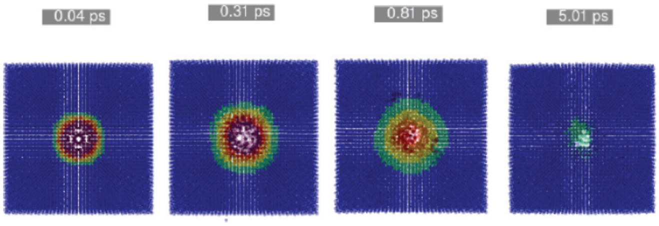

FIG. 2. (Color online) Top view of the thin crystal at 40 fs, 310 fs, 810 fs, and 5 ps after the ionization onset. For color code, see Fig. 1.

From our series of simulations with varying ion trail lengths, we find that the final temperatures of the equilibrated targets are around 200 (430, 900) K for the thin (middle, thick) target. This nicely corresponds to the energy input, Sec. II, which gives 217 (442, 867) K, when applying a specific heat of $3k_B$ per atom. The slight deviations between the final simulated temperatures and the predicted temperatures are mainly due to the energy lost by sputtering. Since the final temperatures are in all cases studied below the melting temperature of LiF, $T_m = 1132$ K, the final crystallite is in its solid state.

We always find the final crystallite to be slightly negatively charged. That is, more Li^+ than F^- ions have left the target. The final charge states are $-5e$ ($-3e$, $-6e$) for the thin (middle, thick) target for a recombination time of 1 ps. Similar values are reached for all ionization times $\geqslant$100 fs, with no statistically relevant difference between the three targets. For the smallest recombination time, 50 fs, the charge state doubles to values of around $-10e$; this is correlated to the higher total sputter yield for $\tau = 50$ fs; see Sec. III C below.

There are two reasons for the negative charge state of the target. (i) During the recombination time, i.e., in the Coulomb explosion phase, mainly particles from the ion trails will be sputtered; these are all positively charged, Li^+ and F^+. (ii) In the later phase, Li^+ has a higher chance to be emitted than F^- due to its smaller mass.

Figure 3 shows the time evolution of density, pressure, and temperature in the track region. For analysis purposes we define this as a cylinder around the ion path with radius $R_{\text{track}} = 6$ Å; we average these quantities inside this region. Temperatures are extremely high immediately after passage of the swift ion. Strictly speaking at these early times, it is not possible to talk about a temperature since the system is in strong nonequilibrium. The high temperature values here thus simply indicate the strong kinetic energies which the ions have received. In the trail volume, temperatures then quickly equilibrate, within a time of a few ps. The final temperatures

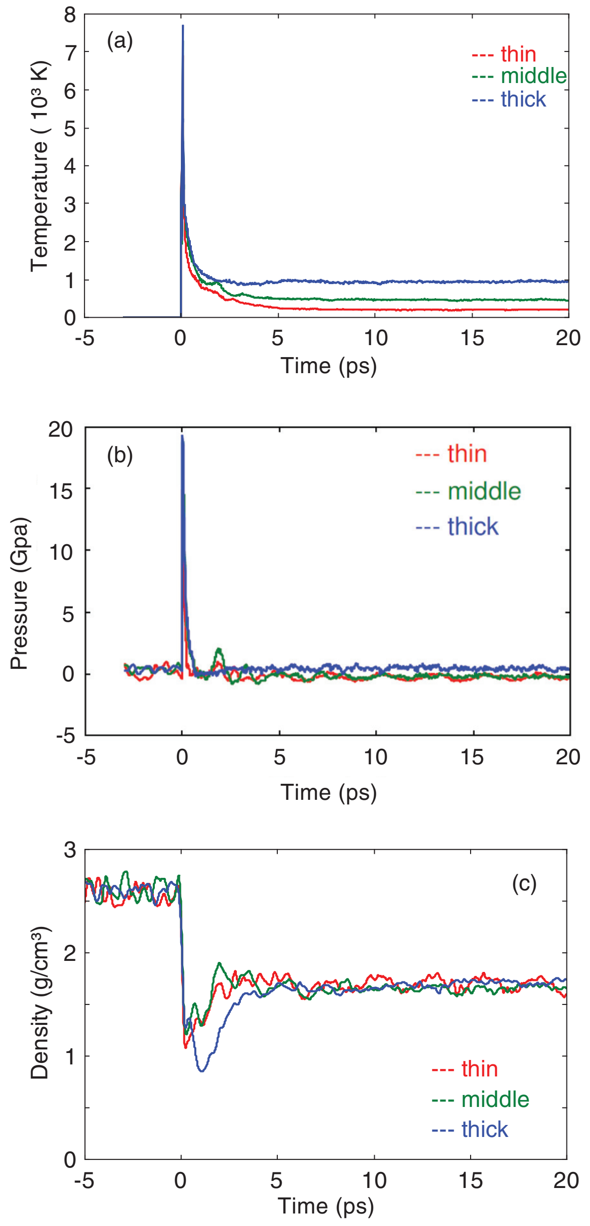

FIG. 3. (Color online) Temporal evolution of (a) temperature, (b) hydrostatic pressure, and (c) density in the track region. Data are averaged throughout the volume of a cylinder with radius $R_{\text{track}} = 6$ Å. Recombination time $\tau = 50$ fs. The three different crystals investigated are denoted as thin, middle, and thick crystal, respectively; see Sec. II D.

correspond to those mentioned above as average temperatures for the entire crystallite. Note that thermalization lasts longest in the thin crystal; this is due to the fact that for this geometry the simulation crystallite has also its widest lateral extension.

Figure 3(b) shows the hydrostatic pressure in the trail region, i.e., the average over all diagonal stress components parallel and perpendicular to the ion track. Initially, immediately after passage of the swift ion, the pressure is high, corresponding to the high energy input. Due to the small lateral sample sizes the pressure can quickly relax. Subsequently, the pressure induces acoustic oscillations in the crystal, which are quickly damped.

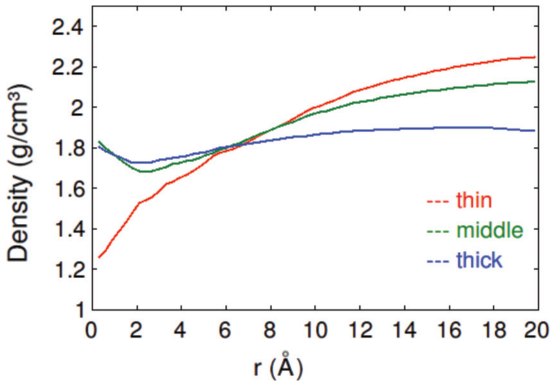

FIG. 4. (Color online) Radial density dependence in the final track structure, at 20 ps.

Most interesting is the evolution of the density in the ion trail region, Fig. 3(c). Density sharply decreases after ionization, but recovers within 1–5 ps and reaches a final constant value of around 60% of the initial density. The initial steep decay is connected to the high compressive pressure building up in the material which leads to the lateral expansion of the trail region; in addition material is sputtered from the surface, again decreasing the density. Density increases again when the pressure pulse, which has been emitted in radial direction, has relaxed the compressive pressure and material can flow back towards the track core. Similar results for the pressure wave have been found earlier in other materials, such as Lennard-Jones-bonded targets.[11,17,18]

Note, however, that our results have been obtained for freestanding crystallites; the density drop obtained must therefore be expected to depend on the lateral crystal size. Indeed, in the thick crystal—which is also the narrowest—the density drop is most pronounced, and the relaxation time of the density is longest. The good agreement of the density evolution for the middle and the thin target show that here the lateral confinement of the track region is strong enough to lead to a stable evolution.

Figure 4 displays the radial dependence of density around the ion trail region at the end of the simulation. Even at a distance of 2 nm from the ion trail the densities do not recover the initial density of 2.5 g/cm^3. The reason hereto is that the material may expand sideways in all cases, since these are freestanding crystallites. No sharp structure can be identified, which separates the final track from the surrounding material. This is in contrast to other materials, such as silica,[15] where a core-shell structure can be identified and the amorphous track core can be clearly distinguished—also by density—from the outer undisturbed material. Our results show how the underdense central region smoothly connects to the adjacent region; density continuously increases. Note that the density at 2 nm distance from the track continuously increases with increasing lateral size of the crystallites; this shows the influence of the lateral confinement.

The thin crystal shows the smallest density close to the ion trail at the time of 20 ps. A comparison with Fig. 3(c)—which shows the density averaged inside the track radius of $R_{\text{track}} = 6$ Å—demonstrates, however, that this is a fluctuation;

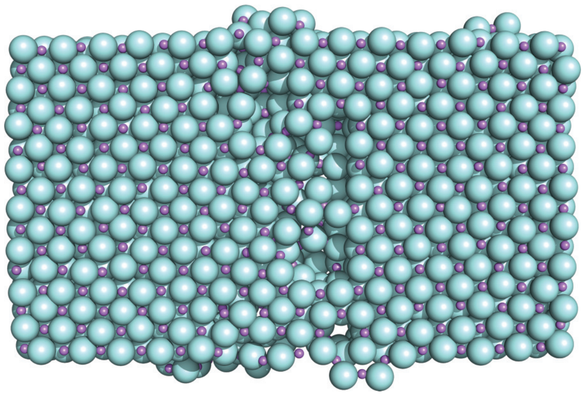

FIG. 5. (Color online) Cross-sectional view through the middle crystal at 20 ps after swift-ion passage showing the strongly disturbed crystal structure in the ion track. Big circles: F^-, small circles: Li^+.

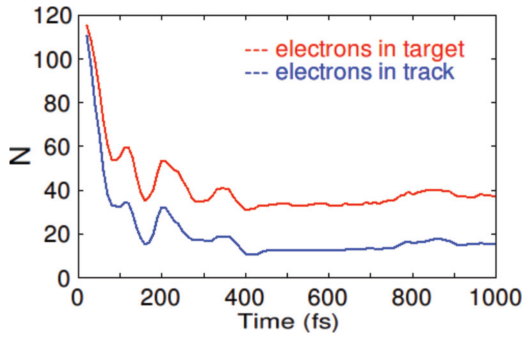

FIG. 7. (Color online) Temporal evolution of the number of electrons in the track, and in the entire target. The track region is taken as a cylinder with radius $R_{\text{track}} = 6$ Å. Data refer to the thick target and $\tau = 1$ ps.

averaged over the times of 5–20 ps the densities in the track region are similar for all three crystals studied.

Figure 5 shows a cross-sectional view of the final track structure. The crystalline structure in the ion track region is strongly distorted, and a high number of defects have been created and frozen in after cooling from the melt. The physical reason for the low track density can hence be attributed to the high defect density in the track core region.

B. Behavior of electrons

Figure 6 displays the electric potential established around the ionization track, immediately after ionization, and 10 fs later. The potential is due to both the ionization of F^- to F^+ in the trail cylinder, and to the electrons which may have left the trail region. Immediately after ionization, the potential reaches maximum values of around 70 V in the trail center. Within 10 fs the potential has smoothed out, and the maximum values are now only around 40 V. This is due to the reaction of the ions to the strong Coulomb fields. In fact our simulations show that the average distance of ions covered during the first 10 fs amounts to 0.7 Å. This motion is a direct sign of the Coulomb explosion happening and shows how quickly ions can respond to the field. The electrical potential, and hence electrical field, extends only several nanometers out of the track region.

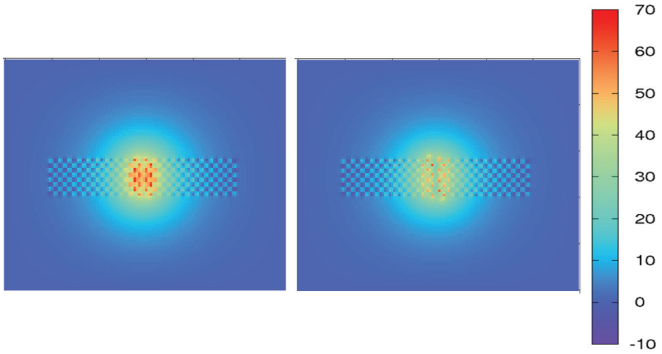

FIG. 6. (Color online) Side view of the thin crystal just after ionization (left) and 10 fs later (right). Color denotes the electric potential (in volts); see color bar at right. The ionization trail is in the middle of the crystal, running from top to bottom. The location of the crystal is visible due to discrete PIC cells.

Figure 7 shows the reaction of the electrons by displaying the number of electrons found in the target and in the track region. Here the thick target has been chosen in which initially 128 electrons have been excited. Here it takes times of around 400 fs until the number of electrons in the target has stabilized; before this time, electrons leave the target. Eventually only 40 electrons (30%) remain in the target and only 15 electrons (12%) remain in the highly positively charged trail region. For the thinner slabs, even fewer electrons remain in the target, only 22% or 14%, for the middle and the thin target.

The electrons that remain in the track region will partly compensate the ionic charges. Figure 8 displays these compensating or screening charges around the F^+ ions. Both the average and the maximum screening charge around the F^+ ions have been plotted. To calculate these numbers, the electron density in a volume of $\Omega = 8.15$ Å^3 around the F^+ ion has been taken into account. Interestingly, screening is only sizable in the first 50 fs. This corresponds to Fig. 7 which shows that electrons quickly leave the target and the trail region. In these first 50 fs, screening can be sizable and completely compensate the ion charge. However, on average, only around 10% of the ion charge is compensated. These values apply for the thick target in which the number of excited electrons is also largest. For the thin and middle target, screening is negligible. Note also that after the first 50 fs, where the target has mostly been depleted of electrons, the effect of screening is minor.

Thus Fig. 8 demonstrates that the role of the electrons is not as decisive as might have been anticipated. They slightly quench the Coulomb explosion, but only very early in the process. This conclusion is of course strongly dependent on the temperature which electrons assume. For lower temperatures, the electrons will stay more closely confined to the track region. As discussed in Sec. II D above, then, the classical, fluid scenario of electron behavior which underlies our PIC strategy fails, and more refined methods of calculating the electron dynamics—for instance based on a Monte Carlo approach—have to be applied.

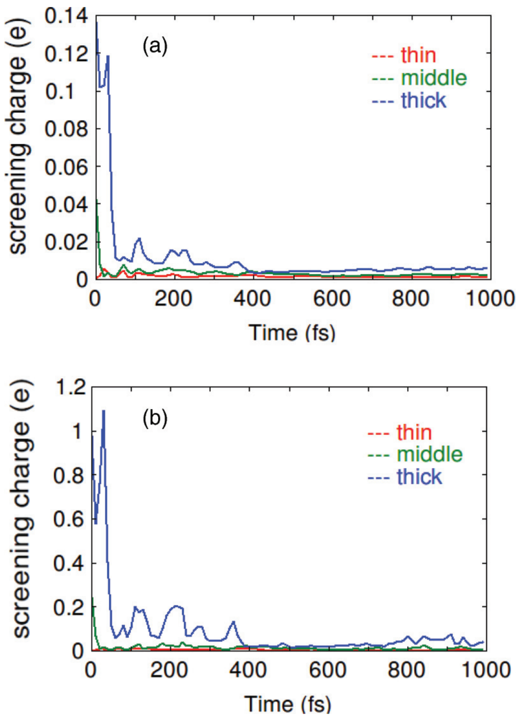

FIG. 8. (Color online) (a) Average and (b) maximum screening charge around F^+ ions. Data refer to a recombination time of $\tau =$ 1000 fs.

Figure 6 allows us to estimate the field strengths which act on the surface of the crystal in the ion trail region; they amount to around 10^{10} V/m. At an electron temperature of 8 eV, the average electron velocity is around 2×10^6 m/s; at these field strengths, electrons, which have been emitted from the track, return within 2 fs from the vacuum to the crystal surface. Since our PIC model does not explicitly resolve the electron dynamics—but assumes that electrons instantaneously adapt their density to the electric potential—this means that our simulation is valid for times >2 fs. This is also about the size of our molecular dynamics time step, 1 fs. We conclude that for the problem that we study here, our PIC approach is valid for processes occurring on a time scale >2 fs, and hence is well applicable to our study.

C. Sputtering

The sputtering from an ion track in LiF has been studied previously as a function of the recombination time τ.[30] The main results were as follows:

(i) Sputter yields decrease with τ. They are highest for a recombination time of $\tau = 50$ fs and reach values around 40; sputter yields decrease towards $Y = 15$ for $\tau = 1$ ps.

(ii) Sputtering is largest for small recombination times, since the LiF crystal becomes energetically disturbed at two times, at $t = 0$ and at $t = \tau$; when the recombination at $t = \tau$ occurs while the system is still in strong nonequilibrium due to the ionization event at $t = 0$, maximum perturbation of the atomic system and hence sputtering occurs.

(iii) When τ becomes even smaller than 50 fs, the sputter yield must vanish. Our simulations show that sputtering occurs as soon as $\tau > 10$ fs.

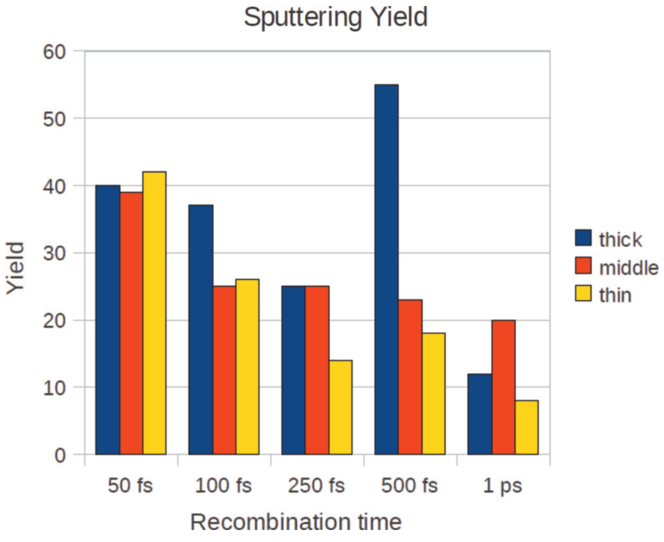

FIG. 9. (Color online) Sputtering yield for different recombination times.

(iv) Fast ions are emitted early. This group of sputtered particles also includes the Coulomb explosion part.

(v) The energy distribution of sputtered ions consists of two groups: a low-energy group centered at <1 eV and a high-energy group at 7–8 eV.

Here we wish to report on the influence of the system size—in particular of the trail length—on the sputtering behavior. While experiments on freestanding LiF films of such small thicknesses as studied here may not be easily performed experimentally, our results may apply to the sputtering from ultrathin LiF films grown on a substrate. They may also be used as a model for intermittent tracks; in these the impinging swift ion does not form one continuous ionization trail, but rather a series of smaller trails. In this study we vary the extension of these ionization trails.

Figure 9 shows the sputtering yield for the three target geometries and various recombination times. We see that the main trend of a decreasing sputter yield with increasing ionization time holds well for all three track lengths studied. The exception for the thick target for $\tau = 0.5$ ps is a statistical excursion. In all cases part of the emitted ions returns to the surface due to the strong attractive forces and the near-surface electrical fields; in the case mentioned substantially fewer emitted ions return to the surface, thus enhancing the net sputter yield.

Figure 10 shows the energy and angular distribution of sputtered particles. Again these results are independent of the track length of the system. The energy distribution features the 2-group structure mentioned in item (v) above. The angular distribution shows strongly anisotropic emission centered in a cone with opening angle of 60° around the surface normal.

A more detailed analysis of the sputtering process is revealing for the nature of the Coulomb explosion process occurring. For the middle target and the smallest recombination time, $\tau = 50$ fs, we find a sputter yield of $Y = 39$ ions. During the ionization period, 4 fast Li^+ ions are sputtered; until 300 fs, another 4 Li^+ ions are ejected. In the ensuing time, mostly cluster ions and neutral LiF molecules are ejected; the largest cluster is a $(Li_7F_6)^+$ ion. The results are similar for the largest

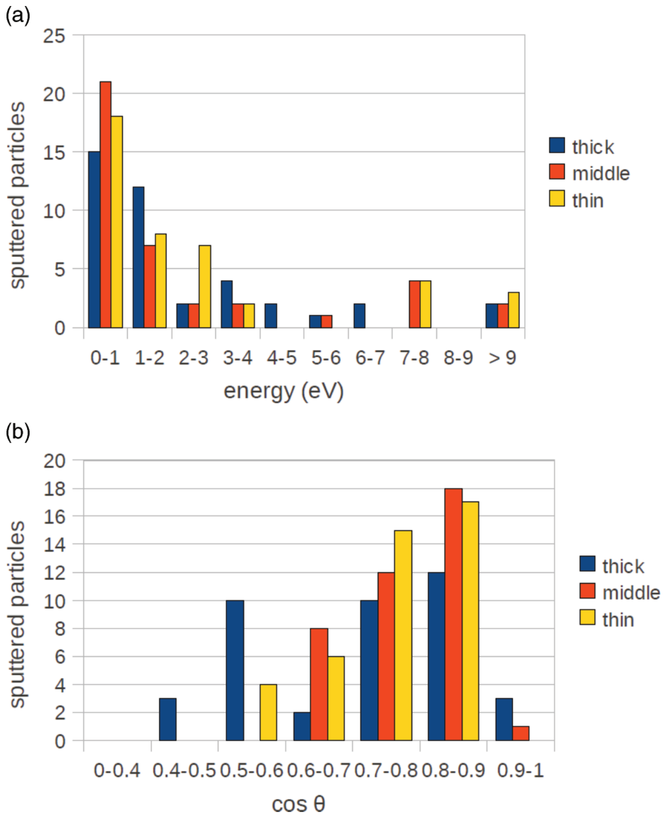

FIG. 10. (Color online) (a) Energy and (b) angular distribution of sputtered particles for the recombination time 50 fs. θ denotes the polar emission angle with respect to the surface normal; $\cos\theta = 1$ corresponds to emission perpendicular to the surface.

recombination time, $\tau = 1$ ps, $Y = 20$. Here again Li^+ ions are emitted early (within 50 fs) followed by emission of cluster ions and neutral molecules.

So we conclude that sputtering occurs in several batches:

(1) During the Coulomb explosion phase, immediately after the passage, mostly single ions, and in particular the light Li^+, are sputtered.

(2) Recombination again injects energy into the system, leading to further emission of monomeric ions.

(3) Later, neutral LiF molecules and polyatomic cluster ions dominate the emission process.

In experiment, often oblique ion impacts are performed. We can compare our results for perpendicular ion incidence with simulations for oblique incidence. In these experiments it is observed that particle emission features a jet perpendicular to the surface even for oblique incidence. While the statistical basis of our simulations is not very rich, we also observe emission patterns which do not favor the incident ion cylinder axis but rather point to a jet in the normal direction. We argue that the reason hereto lies in the electric field established in the target, which is directed normal to the surface and acts during the emission process.

IV. CONCLUSIONS

We formulated a hybrid PIC/MD scheme to model the processes occurring in a LiF crystal after electronic excitation by a swift ion. It allows to understand the processes of Coulomb explosion and charge screening occurring in the crystal immediately after swift-ion passage. We model the time during which free electrons are available by a single parameter, the recombination time of the excited free electrons.

While the molecular dynamics part gives a complete picture of the ion dynamics, the electron part is restricted. (i) We do not implement a full electron dynamics; this appears uncritical since electrons adapt on a time scale of a few fs to the ambient potential distribution. (ii) Electrons are treated as a classical fluid; all kinetic electronic processes (electron collisions, impact ionization, Auger decay, etc.) are disregarded. Their inclusion would be possible in a Monte Carlo (MC) model of electron transport; up to now, a consistent MD/MC model of ion tracks has not been set up. In this sense, our model is not meant to give a fully realistic quantitative prediction of the processes occurring after swift-ion passage through a LiF crystal; rather it is meant to assess the importance of electron dynamics on the nonequilibrium processes occurring in the ionic system.

We find the following:

(1) Within the first 50 fs, a Coulomb explosion is seen in the ion trail. Its most prominent effect is the emission of fast (7–8 eV) Li^+ ions from the solid. It is caused by electrical fields at the target surface of the order of 10^{10} V/m. The target is left behind in a negative charge state.

(2) After a few hundred fs, monatomic ion emission becomes rare and is supplanted by the emission of neutral molecules and polyatomic cluster ions.

(3) In the target, the huge deposited energy density leads to a high thermoelastic pressure, which starts a pressure wave in radial direction. These processes are similar to those found in track studies of nonionic materials.

(4) The resulting track has a density of around 60% of the original LiF density and consists of highly defective material.

(5) Electrons partly shield the positive ions in the track; for the electron temperature considered here (8 eV) the shielding was, however, minor (10% on the average), and occurred mainly in the first 50 fs of the process. This suggests that a modeling of the ion track without the inclusion of the electrons should give a valuable zeroth order approximation.

(6) The effect of the ion recombination time, which we varied between 50–1000 fs, is only minor. The track structure only marginally changes, while the sputtering even decreases. The reason hereto lies in the fact that the energy input by recombination is most efficient if it occurs promptly after ionization.

ACKNOWLEDGMENT

This work was supported by the Carl Zeiss foundation.

---

[*] urbassek@rhrk.uni-kl.de; URL: http://www.physik.uni-kl.de/urbassek/

[1] R. L. Fleischer, P. B. Price, and R. M. Walker, *Nuclear Tracks in Solids* (University of California, Berkeley, 1975).

[2] W. Assmann, M. Toulemonde, and C. Trautmann, in *Springer Topics in Applied Physics*, edited by R. Behrisch and W. Eckstein, Vol. 110 (Springer-Verlag, Berlin, 2007), pp. 401–408.

[3] M. Toulemonde, W. Assmann, C. Trautmann, and F. Grüner, Phys. Rev. Lett. **88**, 057602 (2002).

[4] M. Toulemonde, W. Assmann, C. Dufour, A. Meftah, F. Studer, and C. Trautmann, in *Ion Beam Science: Solved and Unsolved Problems*, Vol. 52 of Mat. Fys. Medd. Dan. Vid. Selsk., edited by P. Sigmund (Royal Danish Academy of Sciences, Copenhagen, 2006), p. 263.

[5] G. Schiwietz, K. Czerski, M. Roth, F. Staufenbiel, and P. L. Grande, Nucl. Instrum. Meth. B **226**, 683 (2004).

[6] P. Sigmund, R. Bimbot, H. Geissel, H. Paul, and A. Schinner, J. of the ICRU **5**, 1 (2005).

[7] P. Sigmund, in *Ion Beam Science: Solved and Unsolved Problems*, Vol. 52 of Mat. Fys. Medd. Dan. Vid. Selsk., edited by P. Sigmund (Royal Danish Academy of Sciences, Copenhagen, 2006), p. 557.

[8] B. Gervais and S. Bouffard, Nucl. Instrum. Meth. B **88**, 355 (1994).

[9] M. Beuve, M. Caron, B. Gervais, H. Rothard, A. Clouvas, and C. Potiriadis, Eur. Phys. J. D **15**, 293 (2001).

[10] M. P. R. Waligorski, R. N. Hamm, and R. Katz, Nucl. Tracks Radiat. Meas. **11**, 309 (1986).

[11] H. M. Urbassek, H. Kafemann, and R. E. Johnson, Phys. Rev. B **49**, 786 (1994).

[12] E. M. Bringa and R. E. Johnson, Nucl. Instrum. Meth. B **143**, 513 (1998).

[13] E. M. Bringa and R. E. Johnson, Nucl. Instrum. Meth. B **180**, 99 (2001).

[14] P. Kluth, C. S. Schnohr, O. H. Pakarinen, F. Djurabekova, D. J. Sprouster, R. Giulian, M. C. Ridgway, A. P. Byrne, C. Trautmann, D. J. Cookson *et al.*, Phys. Rev. Lett. **101**, 175503 (2008).

[15] O. H. Pakarinen, F. Djurabekova, K. Nordlund, P. Kluth, and M. C. Ridgway, Nucl. Instrum. Meth. B **267**, 1456 (2009).

[16] A. A. Leino, O. H. Pakarinen, F. Djurabekova, and K. Nordlund, Nucl. Instrum. Meth. B **282**, 76 (2012).

[17] M. Beuve, N. Stolterfoht, M. Toulemonde, C. Trautmann, and H. M. Urbassek, Phys. Rev. B **68**, 125423 (2003).

[18] S. Mookerjee, M. Beuve, S. A. Khan, M. Toulemonde, and A. Roy, Phys. Rev. B **78**, 045435 (2008).

[19] R. E. Johnson and J. Schou, Mat. Fys. Medd. K. Dan. Vidensk. Selsk. **43**, 403 (1993).

[20] E. M. Bringa and R. E. Johnson, Phys. Rev. Lett. **88**, 165501 (2002).

[21] D. A. Young, Europhys. Lett. **59**, 540 (2002).

[22] D. A. Young, Nucl. Instrum. Meth. B **225**, 231 (2004).

[23] D. A. Young, Nucl. Instrum. Meth. B **252**, 175 (2006).

[24] Y. Zhang, Y. Wang, and W. J. Weber, Nucl. Instrum. Meth. B **286**, 1 (2012).

[25] L. W. Hobbs, F. W. Clinard, S. J. Zinkle, and R. C. Ewing, J. Nucl. Mater. **216**, 291 (1994).

[26] J.-M. Delaye and D. Ghaleb, Mat. Sci. Eng. B **37**, 232 (1996).

[27] B. P. Uberuaga, R. Smith, A. R. Cleave, F. Montalenti, G. Henkelman, R. W. Grimes, A. F. Voter, and K. E. Sickafus, Phys. Rev. Lett. **92**, 115505 (2004).

[28] R. Devanathan, P. Durham, J. Du, L. R. Corrales, and E. M. Bringa, Nucl. Instrum. Meth. B **255**, 172 (2007).

[29] E. M. Bringa, S. O. Kucheyev, M. J. Loeffler, R. A. Baragiola, A. G. G. M. Tielens, Z. R. Dai, G. Graham, S. Bajt, J. P. Bradley, C. A. Dukes *et al.*, Astrophys. J. **662**, 372 (2007).

[30] Y. Cherednikov, S. N. Sun, and H. M. Urbassek, Nucl. Instrum. Meth. B (to be published, 2013).

[31] C. K. Birdsall, IEEE Trans. Plasma Sci. **19**, 65 (1991).

[32] C. K. Birdsall and A. B. Langdon, *Plasma Physics via Computer Simulation* (McGraw-Hill, New York, 1991).

[33] R. W. Hockney and J. W. Eastwood, *Computer Simulation using Particles* (IOP, Bristol, 1994).

[34] B. Briehl and H. M. Urbassek, Surf. Coat. Technol. **160**, 259 (2002).

[35] C. Jungreuthmayer, M. Geissler, J. Zanghellini, and T. Brabec, Phys. Rev. Lett. **92**, 133401 (2004).

[36] C. Jungreuthmayer, L. Ramunno, J. Zanghellini, and T. Brabec, J. Phys. B **38**, 3029 (2005).

[37] N. A. Inogamov, A. Y. Faenov, V. A. Khokhlov, V. V. Zhakhovskii, Y. V. Petrov, I. Y. Skobelev, K. Nishihara, Y. Kato, M. Tanaka, T. A. Pikuz *et al.*, Contrib. Plasma Phys. **49**, 455 (2009).

[38] Y. Cherednikov, N. A. Inogamov, and H. M. Urbassek, J. Opt. Soc. Am. B **28**, 1817 (2011).

[39] W. H. Press, S. A. Teukolsky, W. T. Vetterling, and B. P. Flannery, *Numerical Recipes in C* (Cambridge University Press, Cambridge, 1992), 2nd ed.

[40] C. J. Fennell and J. D. Gezelter, J. Chem. Phys. **124**, 234104 (2006).